SCIEPublish

Article

Motion Control of Floating Wind-Wave Energy Platforms

Shuang-Rui Yu, Zhi-Ming Yuan * and Atilla Incecik

Department of Naval Architecture, Ocean and Marine Engineering, University of Strathclyde, Glasgow G4 0LZ, UK; shuangrui.yu@strath.ac.uk (S.-R.Y.); atilla.incecik@strath.ac.uk (A.I.)

* Corresponding author. E-mail: zhiming.yuan@strath.ac.uk (Z.-M.Y.)

Received: 21 December 2024; Accepted: 4 February 2025; Available online: 12 February 2025

ABSTRACT: Mitigating wave-induced motions in floating multi-body systems is a critical challenge in ocean engineering. For single floating structures, such as floating platforms or vessels, applying active control requires considerable energy. It is also a common solution to add auxiliary structures and a power take-off (PTO) device, thereby forming a multi-body system that utilises passive control. However, the effectiveness of this method is limited due to varying phase differences between control forces and motions, which change across different wave frequencies. The present work proposes a novel semi-active structural control method, which can effectively provide optimised control force to the main body within a multi-body system. The key point of this method is tuning the phases between the forces and motions of floating bodies. Proper tuning can neutralise the main floating body's wave-induced motion by utilising the wave-induced motion of the auxiliary structure. The controller is developed under an optimal declutching control framework, adjusting the damping coefficients of the PTO system to provide discrete resistance to the target body. A floating semi-submersible (SS) platform equipped with a heave ring as an auxiliary structure is selected and analysed as the case study. The results demonstrate the method's efficacy in reducing motion for floating wind turbine (FWT) platforms and its applicability to various types of multiple floating bodies. Interestingly, our optimal declutching control can "kill two birds with one stone". It can simultaneously enhance motion reduction and increase power capture. In the current study, the proposed controller achieved a maximum motion reduction of 30% for the platform.

Keywords: Floating wind turbine; Floating wind-wave energy platform; Motion control; Semi-active control; Power take-off (PTO) system

1. Introduction

The implementation of floating structures in deep-sea environments is a contemporary trend in ocean engineering, as it offers more wind or wave energy storage and less noise and visual pollution. One of the most challenging problems in deep-sea environments is the control of wave-induced motion in floating bodies [1]. Wave-induced motion can cause significant instability and even damage to offshore structures, leading to high maintenance costs and decreased operational efficiency. For Floating Offshore Wind Turbines (FOWTs), the wave-induced motions will cause the reduction of blade swept area and, hence, the power output. In the case of spar-type FOWT, the dominant pitch motion may induce significant bending moments of the tower and potential oil leaks. Furthermore, according to regulations [2], the acceleration at the nacelle should be less than 0.3 g to avoid damage to the power train during operation.

Ocean engineering has traditionally focused on optimising the shapes of floating bodies and implementing passive control methods to reduce wave-induced motions. The optimised designs are also single bodies. Fixed heave plates can add additional mass and suppress the heave motion of floating bodies [3–5]. Helical strakes are designed to suppress vortex-induced vibration (VIV) [6–9]. Truss spar is a concept designed to increase the effective vertical mass and heave damping of the structure and hence reduce the motion of floating platforms [10,11]. However, the effect of designs depends on the floating structure geometry and the excitation force conditions. Additionally, the shape optimisation process can be computationally expensive, as it often requires extensive simulations and iterative refinement.

Passive control methods also have been widely employed to reduce wave-induced motions, but their effectiveness varies depending on the application. Passive control methods, such as movable heave plates, mooring systems, tuned

mass damper (TMD) [12], tuned liquid column damper (TLCD), and tuned liquid column ball damper (TLCBD), can be effective in certain scenarios [13,14]. Mooring lines could also be considered a passive control method. Du et al. analysed the performance of offshore floating photovoltaics (FPV) arrays in shallow water and six types of configurations of their mooring lines [15]. In this study, the key performance is not the motion but the maximum mooring tension at the fairlead. However, these passive control methods are highly sensitive to the wave conditions and only effective in a narrow wave bandwidth.

Active control methods are state-of-the-art solutions to reduce wave-induced motions in floating structures. Blade pitch control is one of the typical active control methods for floating wind turbines to maximise the extraction of wind energy and reduce the fluctuation of power output [16]. It can also be applied to mitigate waved-induced motion, but it has to balance the weightings of the two objectives [17,18]. Moreover, such a method that relies on modifying the aerodynamic lift on the blades is incapable of operating during shutdowns due to extreme events when load mitigation may be most critical. Furthermore, wave frequency is much higher than the frequency at which wind speed or wind direction changes. Frequent blade pitching is harmful to the rotor's gear and bearing system. This method primarily impacts the blade loads [19] and leads to negative damping of the platform-pitch mode [16].

Some other active control methods using additional structures are proposed for floating structures' motion control, including active dampers, active vertical vanes, active moorings, and gyroscopes [20–23]. While these technologies have demonstrated their ability to improve motion control, they often necessitate additional power input, increasing energy consumption [24]. Furthermore, the implementation of these active control methods can require complex control algorithms and hardware, potentially increasing the overall cost and maintenance requirements of the system.

This paper is part of the author's PhD thesis titled "Control on Multiple Floating Bodies" at the University of Strathclyde. In this paper, we propose a novel approach that utilises wave energy itself to control the motion induced by waves, thereby minimising and even eliminating the need for extra power input. The proposed method involves connecting a floating heave ring to a floating semi-submersible (SS) wind energy platform, creating a multi-body system that can be actively tuned to reduce the motion of the primary floating body effectively. The detailed concept designs are shown in Section 2. This is achieved through the implementation of an optimal declutching control method, which was proposed in the research of Yu et al. [25]. This method tunes the total force acting on the bodies, ultimately reducing the motion experienced by the primary floating body. The proposed multi-body control method can be regarded as a semi-active method, which controls some tuneable parameters (e.g., stiffness or damping) without needing as much energy input as active systems.

The paper is organised as follows. Section 2 describes the numerical modelling of the novel SS-ring system. Section 3 introduces the hydrodynamics, constraint matrix method, and state-space representation of the floating multi-body system. Section 4 introduces the control algorithm applied to the floating multi-body system. Section 5 discusses the optimal control results of the SS-ring system. Finally, conclusions are summarised in Section 6.

2. Description of an SS-Ring System

The computational model is the combination of an OC4 semi-submersible platform [26] and a heave ring, as illustrated in Figure 1. The hydrodynamic forces acting on the columns are much larger than on pontoons and cross braces between columns so that these structures can be neglected for simplicity. In most sea areas, wind energy typically has dominant components at frequencies lower than where wave energy becomes large. Since the main objective is to reduce the wave-induced motions, the rotor mounted on the wind turbine tower is fixed, and the coupled dynamics between the wind turbine and platform can be neglected.

The global and body-fixed coordinates are described in a Cartesian coordinate (x, y, and z) as illustrated in Figure 1. The origins of the body-fixed coordinates are located at the centre of gravity of each body, respectively. The primary DoF for the semi-submersible platform's motion is in the heave direction. The water depth is set to 200 m in this case.

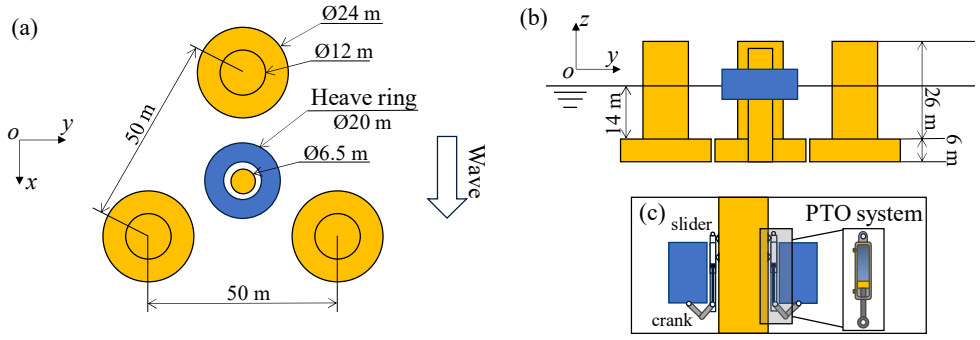

Figure 1. Top view (**a**) and side view (**b**,**c**) of the SS-ring system.

The heave ring works by providing additional hydrodynamic damping to reduce the heave motion of the structure. Traditional heave plates are typically fixed beneath the columns or pontoons of the platform by a truss structure [27,28]. In this case, the heave ring is located at the water surface and surrounds the central column. It is designed to be movable along the z-axis relative to the semi-submersible platform and is connected to the platform with a slide connection. A PTO system is mounted at the central column of the platform and interfaces with the heave ring through a crank and a slider. This linkage transfers the vertical motion of the heave ring to the PTO system. Similar concept was applied in a hybrid Spar-Torus Combination [29].

The parameters of the OC4 semi-submersible platform and the heave ring are presented in Table 1, and the mass Properties are presented in Table 2. SWL is the abbreviation of Still Water Line. Different from the tuned heave plates, the damping coefficient of the damper is not predefined as a constant. Instead, it varies between 0 and B_{PTO} with the current declutching control method.

Table 1. Dimensions of the semi-submersible platform [26] and ring.

Parameters	Dimensions
Depth to platform base below SWL (total draft)	20 m
Elevation of main column (tower base) above SWL	10 m
Elevation of offset column above SWL	12 m
Spacing between offset columns	50 m
Length of upper columns	26 m
Length of base columns	6 m
Depth to top of base columns below SWL	14 m
Diameter of the main column	6.5 m
Diameter of offset (upper) columns	12 m
Diameter of base columns	24 m
Ring outer diameter	20 m
Ring inner diameter	10 m
Ring draft	4 m

Table 2. Mass properties of the semi-submersible platform and ring.

Parameters	Dimensions
Platform mass, including ballast	1.3473×10^7 kg
CM location below SWL	13.46 m
Platform roll/pitch inertia about CM	6.827×10^9 kg·m^2
Platform yaw inertia about CM	1.226×10^{10} kg·m^2
Ring mass	3.8642×10^6 kg
Ring roll/pitch inertia about CM	4.995×10^8 kg·m^2

3. Methodology

The concept of optimal declutching control used on multiple floating bodies was proposed and studied in the research of Yu et al. [25]. Various objective functions and physical scenarios have been discussed in that research. This paper only focuses on the realisation of the motion control of one body in the multi-body system.

3.1. Motion Equation of a Floating Multi-Body System

For a multi-body floating system, the dimensions of the mass matrix, motion vector, and force vector are $6N \times 6N$, $6N \times 1$, and $6N \times 1$, respectively, where N is the number of bodies. The theoretical model of N floating bodies without any connection is depicted in as described in the paper of Yu et al. [25]. The global coordinate $o\text{-}xyz$ is a right-handed Cartesian coordinate with $x\text{-}y$ axes in the horizontal water plane and z axis oriented in the upward direction. Each body can be simplified as a mass point at its centre of gravity (CoG). The surface memory effect related to the shape and velocity of a floating body is described by additional mass and damping coefficients. The hydrodynamic parameters and motion responses are described in body-fixed coordinates $o^j\text{-}x^j y^j z^j$, where j corresponds to the j-th body.

Assuming the flow field is ideal, potential flow theory is applied to derive the hydrodynamic parameters of the floating bodies. The water depth, h, is assumed to be infinite, and the waves propagate towards the positive x-axis throughout the computation. When considering the nonlinear wave surface memory effect, the time-domain motion equation of multiple floating bodies in the regular wave is

$$(\boldsymbol{M}+\boldsymbol{m})\ddot{\boldsymbol{\eta}}(t)+\int_0^t \boldsymbol{h}_{\mathrm{r}}(t-\tau)\dot{\boldsymbol{\eta}}(\tau)d\tau+\boldsymbol{K}\boldsymbol{\eta}(t)=\boldsymbol{f}_{\mathrm{e}}(t)+\boldsymbol{f}_{\mathrm{PTO}}(t) \tag{1}$$

where the hydrodynamic coefficients and excitation wave forces are described in their body-fixed coordinates, respectively. $\boldsymbol{M}$ is the body mass matrix; $\boldsymbol{m}$, which represents $\boldsymbol{\mu}(\infty)$, is the added mass matrix at infinite frequency. $\boldsymbol{h}_{\mathrm{r}}(t)$ is the kernel retardation function matrix; $\boldsymbol{K}$ is the stiffness matrix. $\boldsymbol{\eta}(t)$, $\dot{\boldsymbol{\eta}}(t)$ and $\ddot{\boldsymbol{\eta}}(t)$ are the displacement, velocity and acceleration vectors, respectively, where the motion of body j is defined as $\boldsymbol{\eta}^j=\left[\eta_1^j;\ \eta_2^j;\ \eta_3^j;\ \eta_4^j;\ \eta_5^j;\ \eta_6^j\right]=\left[x^j;\ y^j;\ z^j;\ \varphi^j;\ \theta^j;\ \psi^j\right]$, representing the surge motion, sway motion, heave motion, roll angle, pitch angle, and yaw angle of j-th body, respectively. ${\boldsymbol{f}_{\mathrm{e}}}^j=\left[\zeta^{\mathrm{A}} f_{\mathrm{W}}^j \sin\left(\omega_{\mathrm{W}} t+\varepsilon_i^j\right)\right]^{\mathrm{T}}, i=1,2,\cdots 6$, are the components of the j-th wave excitation force vector, where f_{W} is the wave force transfer function; ζ^{A} is the incoming wave amplitude; ω_{W} is the angular wave frequency; ε_i^j are the phases of harmonic components of a periodic wave.

$\boldsymbol{f}_{\mathrm{PTO}}(t)$ is the PTO damping force vector applied by the PTO unit between adjacent multiple floating bodies, which can be written as

$${f_{\mathrm{PTO}}}^j(t)=-B_{\mathrm{PTO}}^j\dot{\eta}_7^j(t), j=1,2,\cdots,N-1 \tag{2}$$

where B_{PTO}^j is the PTO damping between the adjacent j-th and (j+1)-th floating bodies, which is defined as a constant; $\dot{\eta}_7^j(t)$ is the relative velocity between the adjacent j-th and (j+1)-th floating bodies. The average power output of the system's PTO is defined as

$$P_{\mathrm{PTO}}=\frac{1}{T}\int_0^T[\sum\nolimits_{j=1}^{N-1} B_{\mathrm{PTO}}^j\dot{\eta}_7^j(t)^2]dt \tag{3}$$

In this paper, two floating bodies are considered as an example, and hence, N is set to be 2 herein. The motion Equation (1) of the two-body system is a 12-DoF (Degree of Freedom) equation, where $\boldsymbol{\eta}=\left[\boldsymbol{\eta}_i^1,\boldsymbol{\eta}_i^2\right]^{\mathrm{T}}, i=1,2,\cdots,6$ or represented as $\boldsymbol{\eta}=[x^1,y^1,z^1,\varphi^1,\theta^1,\psi^1,x^2,y^2,z^2,\varphi^2,\theta^2,\psi^2]^{\mathrm{T}}$, representing surge, sway, heave, roll, pitch, and yaw respectively; $f_{\mathrm{PTO}}=-B_{\mathrm{PTO}}\Delta\dot{z}(t)$, where $\Delta\dot{z}(t)$ is the relative heave velocity between the semi-submersible platform and the heave ring herein.

3.2. Approximation of Radiation Term

In the time domain, the nonlinear radiation term in the motion equation can be derived from Cummins' impulse theory [30]. According to Cummins' equation, the radiation force is

$$\boldsymbol{f}^R(t)=\int_0^t \boldsymbol{h}_{\mathrm{r}}(t-\tau)\dot{\boldsymbol{\eta}}(\tau)d\tau \tag{4}$$

where $\boldsymbol{h}_{\mathrm{r}}(t)$ is the retardation kernel function, representing the wave memory effect. $\boldsymbol{h}_{\mathrm{r}}(t)$ can be obtained from the added mass or potential damping in the frequency domain

$$\boldsymbol{h}_{\mathrm{r}}(t)=\frac{2}{\pi}\int_0^{\infty}\omega\left(m-\boldsymbol{\mu}_{\mathrm{r}}(\omega)\right)\sin(\omega t)\,d\omega=\frac{2}{\pi}\int_0^{\infty}\boldsymbol{\lambda}_{\mathrm{r}}(\omega)\cos(\omega t)\,d\omega \tag{5}$$

where $\boldsymbol{\mu}_{\mathrm{r}}(\omega)$ is the added mass in the frequency domain; $\boldsymbol{\lambda}_{\mathrm{r}}(\omega)$ is the added damping in frequency domain. $\boldsymbol{h}_{\mathrm{r}}(s)$, the Laplace transform of $\boldsymbol{h}_{\mathrm{r}}(t)$, can be regarded as the transfer function from the velocity $\dot{\boldsymbol{\eta}}(s)$ to the radiation force $\boldsymbol{f}^{R}(s)$. The presence of this convolution term in Equation (1) poses challenges for controller design and simulation. To substitute the convolution term by frequency domain identification, the transfer function from the velocity $\dot{\boldsymbol{\eta}}(t)$ to the radiation force $\boldsymbol{f}^{R}(t)$ can be approximated and represented in state-space form

$$\begin{aligned}\boldsymbol{f}^{R}(t)&=\boldsymbol{C}_{\boldsymbol{r}}\cdot\boldsymbol{u}(t)\\ \dot{\boldsymbol{u}}(t)&=\boldsymbol{A}_{\boldsymbol{r}}\cdot\boldsymbol{u}(t)+\boldsymbol{B}_{\boldsymbol{r}}\dot{\boldsymbol{\eta}}(t)\end{aligned} \tag{6}$$

The system matrices $\boldsymbol{A}_{\boldsymbol{r}}$, $\boldsymbol{B}_{\boldsymbol{r}}$ and $\boldsymbol{C}_{\boldsymbol{r}}$ are derived by frequency-domain identification (FDI) using the MSS FDI toolbox [31]. Hence, when considering the wave surface memory effect, Equation (1) can be written as

$$\begin{aligned}(\boldsymbol{M}+\boldsymbol{m})\ddot{\boldsymbol{\eta}}(t)+\boldsymbol{C}_{\boldsymbol{r}}\cdot\boldsymbol{u}(t)+\boldsymbol{K}\boldsymbol{\eta}(t)&=\boldsymbol{f}_{\mathrm{e}}(t)+\boldsymbol{f}_{\mathrm{PTO}}(t)\\ \dot{\boldsymbol{u}}(t)&=\boldsymbol{A}_{\boldsymbol{r}}\cdot\boldsymbol{u}(t)+\boldsymbol{B}_{\boldsymbol{r}}\dot{\boldsymbol{\eta}}(t)\end{aligned} \tag{7}$$

The coupling only exists in the heave and pitch DoFs; therefore, only the added mass and damping coefficients in the heave (DoF33) and pitch (DoF55) directions are considered. As illustrated in Figure 2, the identified results for the heave direction could fit well with data extracted from potential flow software, provided that a sufficient polynomial order (fifth or higher) is employed for the approximation. The time-domain motion results obtained through system identification are compared with the frequency-domain results, as discussed later in Section 5, to validate the approximation of the radiation term. Comparing time-domain simulations using the Cummins integral with the system identification model would offer valuable insights into its accuracy and limitations. However, this comparison is beyond the current study's scope and will be addressed in future research.

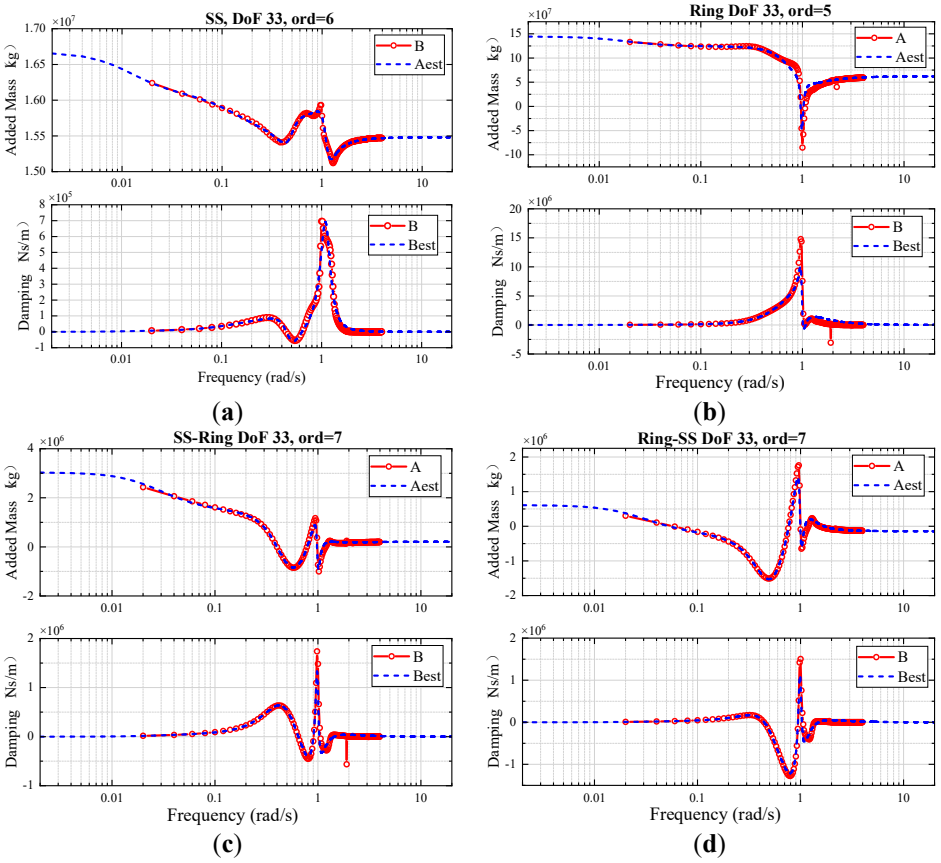

Figure 2. Identification results in heave direction (DoF 33), including added mass and damping for: (**a**) SS platform, (**b**) heave ring, (**c**) cross-interaction from heave ring to SS platform, and (**d**) cross-interaction from SS platform to heave ring.

3.3. Constraint Matrix Method

Within the SS-ring system, the relative motion in z direction remains unrestricted. $f_{\mathrm{PTO}} = -B_{\mathrm{PTO}}\Delta\dot{z}(t)^2$, where $\Delta\dot{z}(t)$ is the relative translational velocity in heave direction between the two bodies herein. Because of the constraints from the slide connection, relative motions in the other directions of the two bodies are the same, except for the heave direction. The relative translation between the two connected bodies can be calculated from the difference between their respective heave motions in the body-fixed coordinate. Therefore, the constraint equations are

$$\begin{cases} x^1 = x^2 \\ y^1 = y^2 \\ z^1 = z^2 + \Delta z \\ \varphi^1 = \varphi^2 \\ \theta^1 = \theta^2 \\ \psi^1 = \psi^2 \end{cases} \tag{8}$$

$$\begin{aligned} \boldsymbol{\eta}^2 = \begin{bmatrix} x^2 \\ y^2 \\ z^2 \\ \varphi^2 \\ \theta^2 \\ \psi^2 \end{bmatrix} &= \begin{bmatrix} 1 & 0 & 0 & 0 & 0 & 0 \\ 0 & 1 & 0 & 0 & 0 & 0 \\ 0 & 0 & 1 & 0 & 0 & 0 \\ 0 & 0 & 0 & 1 & 0 & 0 \\ 0 & 0 & 0 & 0 & 1 & 0 \\ 0 & 0 & 0 & 0 & 0 & 1 \end{bmatrix} \begin{bmatrix} x^1 \\ y^1 \\ z^1 \\ \varphi^1 \\ \theta^1 \\ \psi^1 \end{bmatrix} + \begin{bmatrix} 0 \\ 0 \\ -1 \\ 0 \\ 0 \\ 0 \end{bmatrix} [\Delta z] \\ &= \boldsymbol{S}_{21}\boldsymbol{\eta}^1 + \boldsymbol{S}_{22}\Delta\boldsymbol{z} \end{aligned} \tag{9}$$

where the motions of ring $\boldsymbol{\eta}^2$ can be represented by the motions of semi-submersible platform $\boldsymbol{\eta}^1$ and the relative translation Δz. The matrix form can be rewritten as

$$\boldsymbol{\eta} = \begin{bmatrix} \boldsymbol{\eta}^1 \\ \boldsymbol{\eta}^2 \end{bmatrix} = \begin{bmatrix} \boldsymbol{I} & \boldsymbol{0} \\ \boldsymbol{S}_{21} & \boldsymbol{S}_{22} \end{bmatrix} \begin{bmatrix} \boldsymbol{\eta}^1 \\ \Delta\boldsymbol{z} \end{bmatrix} = \boldsymbol{S} \begin{bmatrix} \boldsymbol{\eta}^1 \\ \Delta\boldsymbol{z} \end{bmatrix} = \boldsymbol{S}\boldsymbol{\eta}' \tag{10}$$

where $\boldsymbol{I}$ is the identity matrix; $\boldsymbol{\eta}'$ is the motion with constraint, and $\boldsymbol{S}$ is the coefficient matrix of constraints. In the motion equation of the connected system, $\boldsymbol{\eta}$, $\dot{\boldsymbol{\eta}}$, $\ddot{\boldsymbol{\eta}}$ can be replaced by $\boldsymbol{\eta}'$, $\dot{\boldsymbol{\eta}}'$, $\ddot{\boldsymbol{\eta}}'$. Substituting Equation (10) to Equation (7), the original 12-DoF equation can be transformed into a 7-DoF equation set

$$\begin{aligned} (\boldsymbol{M} + \boldsymbol{m})\boldsymbol{S}\ddot{\boldsymbol{\eta}}'(t) + \boldsymbol{C}_r \cdot \boldsymbol{u}(t) + \boldsymbol{K}\boldsymbol{S}\boldsymbol{\eta}'(t) &= \boldsymbol{f}_{\mathrm{e}}(t) + \boldsymbol{f}_{\mathrm{PTO}}(t) + \boldsymbol{f}_{\mathrm{h}}(t) \\ \dot{\boldsymbol{u}}(t) = \boldsymbol{A}_r \cdot \boldsymbol{u}(t) + \boldsymbol{B}_r\boldsymbol{S}\dot{\boldsymbol{\eta}}'(t) & \end{aligned} \tag{11}$$

In the global coordinate of the hinge system, the hinge forces are internal forces. In order to eliminate the internal hinge forces $\boldsymbol{f}_{\mathrm{h}}(t)$, multiplies the matrix $\boldsymbol{S}^{\mathrm{T}}$ at both sides of Equation (11). The hinge forces $\boldsymbol{f}_{\mathrm{h}}$ can be eliminated when it multiplies the matrix $\boldsymbol{S}^{\mathrm{T}}$, because in the coordinate system of the hinge system, the hinge forces are internal. According to Newton's third law, the hinge forces and torques of the platform and the heave ring are of equal magnitude and opposite directions. Hence, Equation (11) can be derived as

$$\begin{aligned} \boldsymbol{S}^{\mathrm{T}}(\boldsymbol{M} + \boldsymbol{m})\boldsymbol{S}\ddot{\boldsymbol{\eta}}'(t) + \boldsymbol{S}^{\mathrm{T}}\boldsymbol{C}_r \cdot \boldsymbol{u}(t) + \boldsymbol{S}^{\mathrm{T}}\boldsymbol{K}\boldsymbol{S}\boldsymbol{\eta}'(t) &= \boldsymbol{S}^{\mathrm{T}}\boldsymbol{f}_{\mathrm{e}}(t) + \boldsymbol{S}^{\mathrm{T}}\boldsymbol{f}_{\mathrm{PTO}}(t) \\ \dot{\boldsymbol{u}}(t) = \boldsymbol{A}_r \cdot \boldsymbol{u}(t) + \boldsymbol{B}_r\boldsymbol{S}\dot{\boldsymbol{\eta}}'(t) & \end{aligned} \tag{12}$$

3.4. Performance Indices

Two key performance indices are evaluated in this study: the platform's heave motion and the PTO's power output. Both the performance indices are sensitive to the wave frequency and the damping coefficient of PTO. Figure 3a presents the average heave speed of the semi-submersible platform under different PTO damping coefficients and wave frequencies. The average heave speed is defined as $v_{\mathrm{avg}} = \frac{1}{T}\int_0^T |\dot{z}|dt$. No control is applied to the system herein. Since the SS-ring system is a system with small damping across most wave frequency ranges, the heave results only have an obvious increase near the resonance frequency of 0.62 rad/s. Besides, the heave speed amplifies with B_{PTO}. As B_{PTO} reaches infinity, the platform and ring can be considered welded together. In this situation, the heave speed converges to a constant value.

Another performance index, the time-averaged power absorption of the PTO, is defined as $P_{\mathrm{PTO}} = \frac{1}{T}\int_0^T B_{\mathrm{PTO}}\Delta\dot{z}^2 dt$. Figure 3b shows the average power absorption of the PTO system under different PTO damping coefficients and wave frequencies. The PTO power absorption peaks at a B_{PTO} of 2×10^7 N·s/m. This value is set as the initial B_{PTO} of the PTO system. However, in this paper, the optimisation of P_{PTO} is not our objective and will not be discussed in detail. In the next section, when applying the optimal declutching control method, B_{PTO} will be replaced by B_{d}, which varies over time.

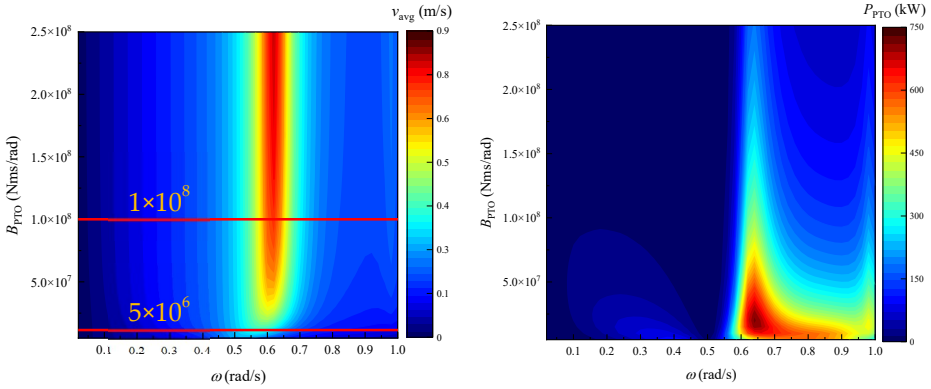

Figure 3. Contour plot of the (**a**) average heave speed of semi-submersible platform, and (**b**) average power absorption of PTO, under different PTO damping coefficients and wave frequencies.

In Section 5, the results and discussions focus primarily on two damping coefficients: 5×10^6 Nms/rad and 1×10^8 Nms/rad, as shown in Figure 3. These two options represent low and high levels of B_{PTO}.

4. Control Theory

4.1. Declutching Control

Phase control is a widely used strategy in active vibration control systems to reduce vibrations by adjusting the phase relationship between forces and velocities. It is also effective for mitigating wave-induced motions in floating structures. This study employs two complementary on-off phase control strategies: latching control and declutching control, both of which use binary control commands to switch between discrete system states.

Latching control provides an infinite damping force alternatively by locking and releasing the floating body with a brake system. The braking effect is similar to a car handbrake, where the brake is applied at zero velocity and relines static friction to prevent motion [32]. Declutching control system provides discrete damping force by switching on and off alternatively the by-pass valve in the circuit of the hydraulic cylinder. When the control command is 0, the by-pass valve is closed, and the damping force is $B_{\mathrm{PTO}}\dot{\eta}_7$; when the control command is 1, the by-pass valve opens, and the damping force is 0.

Define $\boldsymbol{x} = [\boldsymbol{\eta}'(t), \dot{\boldsymbol{\eta}}'(t), \boldsymbol{u}(t)]^{\mathrm{T}}$, the linearised motion response of connected multiple floating bodies can be written as

$$\dot{\boldsymbol{x}} = \gamma \cdot \boldsymbol{x} + \zeta$$

$$\gamma = \begin{bmatrix} \mathbf{0} & \boldsymbol{\Lambda} & \mathbf{0} \\ -\dfrac{\boldsymbol{S}^{\mathrm{T}}\boldsymbol{K}\boldsymbol{S}}{\boldsymbol{S}^{\mathrm{T}}(\boldsymbol{M}+\boldsymbol{m})\boldsymbol{S}} & -\dfrac{\boldsymbol{S}^{\mathrm{T}}\boldsymbol{B}_{\mathrm{d}}\boldsymbol{S}}{\boldsymbol{S}^{\mathrm{T}}\boldsymbol{M}\boldsymbol{S}} & -\dfrac{\boldsymbol{S}^{\mathrm{T}}\boldsymbol{C}_r}{\boldsymbol{S}^{\mathrm{T}}(\boldsymbol{M}+\boldsymbol{m})\boldsymbol{S}} \\ \mathbf{0} & \boldsymbol{B}_r\boldsymbol{S} & \boldsymbol{A}_r \end{bmatrix}, \quad (13)$$

$$\zeta = \begin{bmatrix} \mathbf{0} \\ -\dfrac{\boldsymbol{f}_{\mathrm{e}}(t)}{\boldsymbol{S}^{\mathrm{T}}(\boldsymbol{M}+\boldsymbol{m})\boldsymbol{S}} \\ \mathbf{0} \end{bmatrix}$$

This linearised expression is more suitable for computation and adding a damping force as the control force. The motion equation can be solved using MATLAB's 4th-order Runge Kutta method. Furthermore, the hydrodynamic interactions between multiple bodies induced by wave radiation are also considered.

The damping forces from the resistance of water, the PTO system, and the control system are written in the same term B_{d} in this equation. Define the total declutching control damping coefficient as $B_{\mathrm{d}}(t) = B_{\mathrm{PTO}} + \beta(t)B_{\mathrm{c}}$. When B_{c} is defined as equal to $-B_{\mathrm{PTO}}$, it represents the application of declutching control. With the binary control command β, the linearised representation of the dynamics of the multiple floating bodies will be updated with a new damping force term.

The range of damping of the latching control is from a constant value to infinite; for the declutching control, the range is from 0 to a constant value. Locking the device during the latching periods allows the device to "wait for" the excitation force. Unloading the device during the declutching periods allows the device to "catch up" to the excitation force, which brings the device's velocity (though nonlinear) into phase with the excitation force [32]. The energy costs of declutching control comprise energy consumption of the control system and minor mechanical energy losses due to friction, which are negligible.

4.2. Pontryagin's Maximum Principle

Pontryagin's maximum principle (PMP) is a widely used optimal control theory, suitable for continuous-time systems with smooth dynamics and cost functions. It is particularly useful when the optimal control is a bang-bang or singular control. In this research it can state the way to get the minimum motion of floating bodies in a limited period, from the initial state to the end state with our control.

In order to minimise or maximise the target cost function, we need to minimise or maximise the Hamiltonian, *H*, calculated by the system's state.

$$\begin{aligned} H &= L + \boldsymbol{\lambda}(\gamma \cdot \boldsymbol{x} + \zeta) \\ \dot{\boldsymbol{\lambda}} &= -\frac{\partial H}{\partial \boldsymbol{x}} = -\frac{\partial L}{\partial \boldsymbol{x}} - \boldsymbol{\lambda}\gamma \end{aligned} \tag{14}$$

where $\boldsymbol{\lambda}$ is the Lagrange multiplier and L is the performance index. L can be $\left|v_3^1\right|$ when representing the heave speed of semi-submersible platform, or $B_{\mathrm{PTO}}\dot{z}^2$ when representing the power absorption of PTO. By solving the value of $\boldsymbol{\lambda}$, the Hamiltonian H containing β can be derived. In discrete control, the control command β is binary, which means the command can be either 0 or 1. When the sign of the coefficient before β is negative, β is set to be 0; when the sign is positive, β is 1. If H needs to be maximised, β is defined as

$$\beta = \begin{cases} 0, & \boldsymbol{\lambda}^{\mathrm{T}}(8{:}14)\dfrac{S^{\mathrm{T}}[-\boldsymbol{B}_{\mathrm{c}};\boldsymbol{B}_{\mathrm{c}}]\dot{\theta}}{S^{\mathrm{T}}\boldsymbol{M}S} < 0 \\ 1, & \text{otherwise} \end{cases} \tag{15}$$

If H needs to be minimised, β is defined as,

$$\beta = \begin{cases} 1, & \boldsymbol{\lambda}^{\mathrm{T}}(8{:}14)\dfrac{S^{\mathrm{T}}[-\boldsymbol{B}_{\mathrm{c}};\boldsymbol{B}_{\mathrm{c}}]\dot{\theta}}{S^{\mathrm{T}}\boldsymbol{M}S} < 0 \\ 0, & \text{otherwise} \end{cases} \tag{16}$$

After β is solved, the responses with control can be computed. The responses with control are introduced to the iteration as the initial state until the control command converges and reaches its optimum.

The objective function is defined by the performance index

$$J = \frac{1}{T}\int_0^T L dt \tag{17}$$

The minimisation or maximisation of H corresponds to the same optimum of J. Minimising J implies suppression of the main body's motion through control while maximising J indicates amplification of the main body's motion through control. Different optimisation objectives correspond to different engineering scenarios.

In this paper, the objective is set to minimise the motion of the main floating body in a specified DoF. The objective function to be minimised can be defined as the average L-1 norm as

$$v_{\mathrm{avg}} = \frac{1}{T}\int_0^T |\dot{\eta}| dt \tag{18}$$

where v_{avg} represents the time-averaged speed of the main floating body. The DoF depends on the specific model and scenario. Similarly, the average L-2 norm objective function to be minimised can be defined as

$$v_{\mathrm{avg}} = \frac{1}{T}\int_0^T \dot{\eta}^2 dt \tag{19}$$

The choice of objective function determines the effectiveness of the control.

5. Results and Discussions

The hydrodynamic parameters of the bodies and their interactions are solved in a 3D potential flow solver MHydro [33,34], which uses the Rankine Source method to solve the velocity potential. The MHydro solver computes hydrodynamic coefficients and wave forces. These coefficients are integrated into the mathematical model presented in Section 3 to simulate platform dynamics. Figure 4 demonstrates the validation of the numerical modelling of the heave motion Response Amplitude Operator (RAO) under a regular wave of 1 m. The time-domain heave RAO results strongly agree with the frequency-domain results calculated using potential flow software SESAM. The agreement suggests that simplifying the hydrodynamic coefficients in Section 3.2 is acceptable. Additionally, the difference in motion between the multi-body system (without mechanical connections) and a single SS platform is small, indicating that the hydrodynamic interactions between the bodies are negligible.

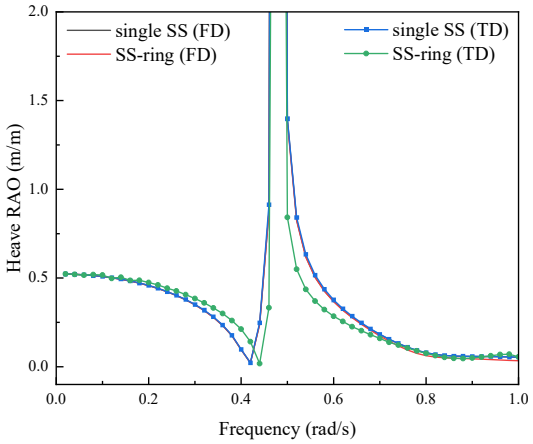

Figure 4. Comparison of heave RAO of a single SS platform and a SS-ring system (FD = Frequency domain, TD = Time domain).

5.1. Control Results in Regular Waves

The objective function to be minimised is the time-averaged heave speed of the semi-submersible platform. Using this objective function, the optimal control command can be calculated in MATLAB with the optimal declutching control method. The initial B_{PTO} is set to 5×10^6 Nms/rad. The heave motions are calculated in wave frequencies range from 0.02–1 rad/s.

In this paper, only the results of the connected multi-body system are discussed. A comparative analysis to determine if these results are better than those of single-body systems is not within the scope of this discussion. In Figure 5, v_{heave} in part of wave frequencies higher than 0.5 rad/s are slightly minimised. The reason is that the declutching control can effectively reduce the average value of B_{PTO}. The peak of the heave response curve moves left. Therefore, the higher frequencies can be optimised. The tendency of P_{PTO} is the same. The peak of the result with a constant B_{PTO} is not accurately presented because of the insufficiently fine interval of wave frequency. The condition when B_{PTO} is 5×10^8 Nms/rad is regarded as welded.

In Figure 5, the controlled result is not as low as the result without damping between 0.4–0.46 rad/s, which means the results are sub-optimal. This is because the PMP can only find local optima. The results with control are highly sensitive to time step, initial state, and final state. This difference is also discussed in the next subsection.

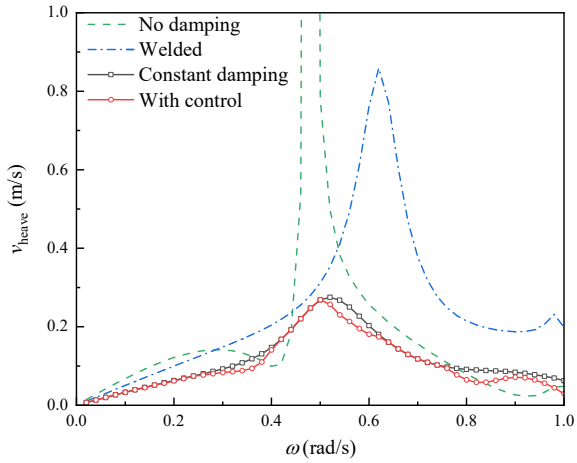

Figure 5. The time-averaged heave speed of the semi-submersible platform in different wave frequencies when B_{PTO} is 5×10^6 Nms/rad (Green dot: No damping; Blue dash: Welded; Black solid: Constant damping; Red solid: With control).

The controlled results with $B_{\mathrm{PTO}} = 1 \times 10^8$ Nms/rad in Figure 6 leads to different conclusions. Comparing Figure 5 and Figure 6 reveals that the heave motion highly depends on the selection of the damping coefficient. The lower damping coefficient configuration (5×10^6 Nms/rad) in Figure 5 reduces heave motion at wave frequencies between 0.5 and 0.6 rad/s, which are above the natural frequency under constant damping (0.52 rad/s). In contrast, a higher damping coefficient configuration (1×10^8 Nms/rad) affects wave frequencies between 0.5 and 0.64 rad/s, which are below the natural frequency under constant damping (0.62 rad/s). This occurs because a high B_{PTO} induces behaviour similar to latching control, allowing the bodies to "wait for" waves at lower frequencies. A high B_{PTO} also enhances the control effect, making the motion reduction percentage higher due to increased energy extraction and greater resistance to motion at specific wave frequencies.

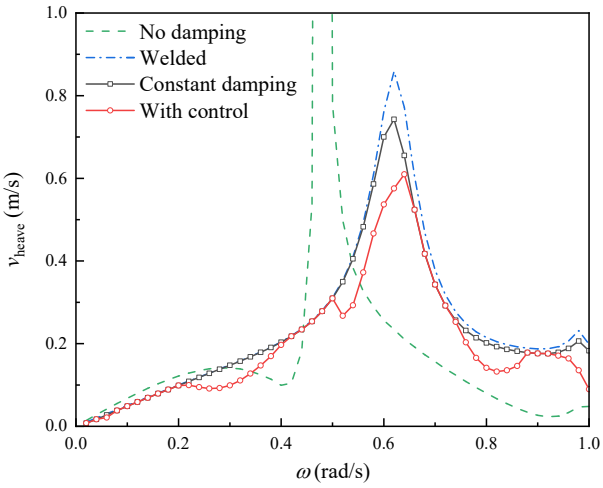

Figure 6. The time-averaged heave speed of the semi-submersible platform in different wave frequencies when B_{PTO} is 1×10^8 Nms/rad (Green dot: No damping; Blue dash: Welded; Black solid: Constant damping; Red solid: With control).

Average value of B_{d} is defined as $\overline{B}_{\mathrm{d}} = \frac{1}{T}\int_0^T B_{\mathrm{d}}(t)dt$, and the result is presented in Figure 7. The value fluctuates with changes in wave frequency but generally remains lower than the initial B_{PTO} due to the nature of the declutching control strategy. The results suggest that while a control command is applied at each wave frequency, leading to a reduction in the average $\overline{B}_{\mathrm{d}}$, this does not necessarily guarantee a significant control effect. The control effect is not solely determined or reflected by $\overline{B}_{\mathrm{d}}$. Therefore, we analyse the time-domain results in the next section for further conclusions.

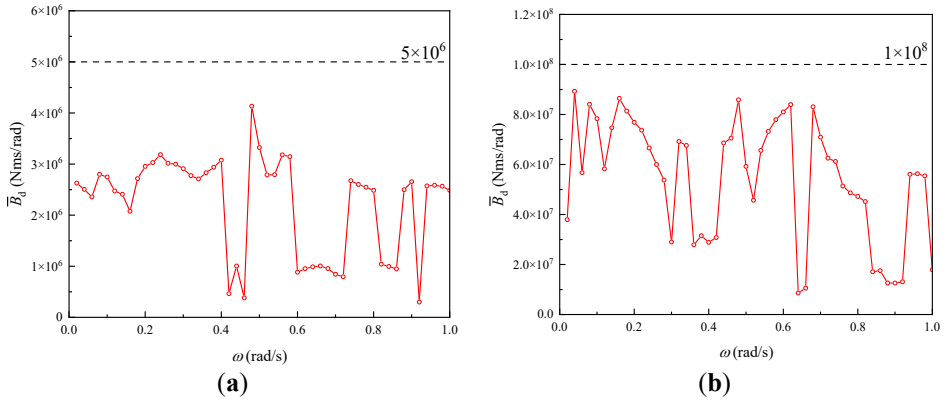

Figure 7. Average value of PTO damping coefficient with control in regular waves when (**a**) $B_{\mathrm{PTO}} = 5 \times 10^6$ Nms/rad and (**b**) $B_{\mathrm{PTO}} = 1 \times 10^8$ Nms/rad.

5.2. Time Domain Analysis

The time-domain results of the platform's heave velocity are shown in Figure 8, along with the corresponding control command β. Generally, the controlled heave velocity is lower than without control, though fluctuations are observed. The control command β is a discrete function with values of 0 and 1, indicating whether the damping force is loaded to the platform.

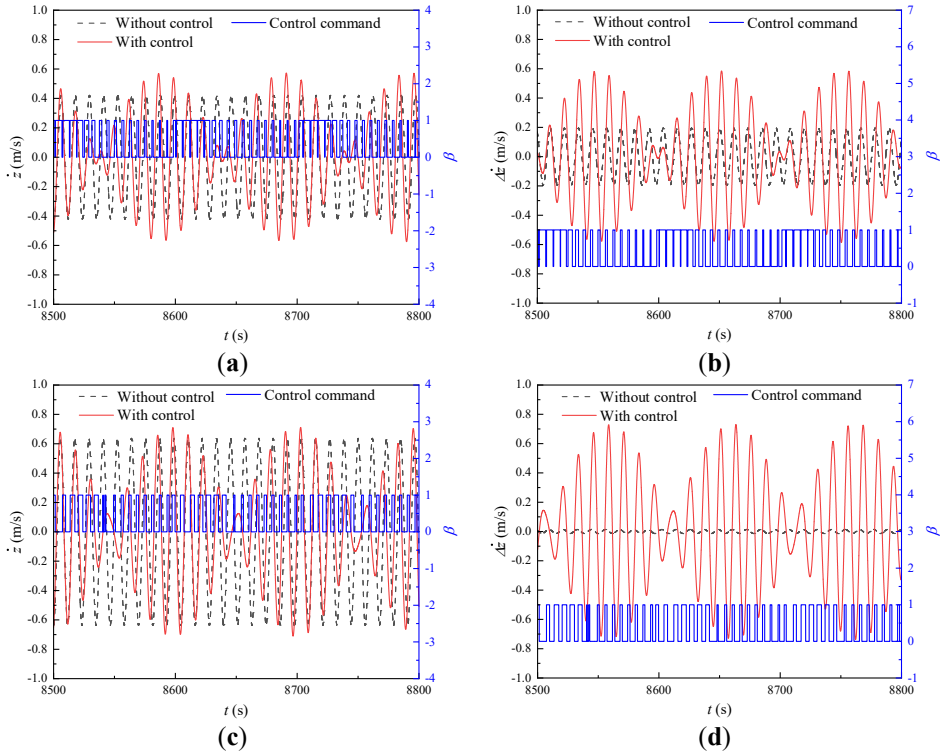

Figure 8. Time domain motion responses and corresponding control command β with $\omega = 0.54$ rad/s: (**a**) $\dot{z}$ at $B_{\mathrm{PTO}} = 5 \times 10^6$ Nms/rad; (**b**) $\Delta\dot{z}$ at $B_{\mathrm{PTO}} = 5 \times 10^6$ Nms/rad; (**c**) $\dot{z}$ at $B_{\mathrm{PTO}} = 1 \times 10^8$ Nms/rad; and (**d**) $\Delta\dot{z}$ at $B_{\mathrm{PTO}} = 1 \times 10^8$ Nms/rad.

The heave ring is relatively large, which provides large hydrodynamic damping to the system. The declutching control significantly reduces the platform's average damping. In an almost undamped system, the controlled motion in the time domain tends to be periodic but not sinusoidal. In Figure 8, the results under control are approximate to the response without damping. The profile of the controlled curve changes to a "beat vibration" pattern, a phenomenon typically observed in forced, undamped oscillations. It is important to note that the system parameters of the semi-submersible platform stay unchanged. Consequently, the observed variation in frequency is attributable to the resultant force of the wave force and the PTO's damping force. As the average $\dot{z}(t)$ of the platform decreases, there is a corresponding reduction in the control time and, conversely, an increase in $\dot{z}(t)$ results in a longer control duration.

While the control implementation results in a reduction of the average $\dot{z}(t)$, it also leads to an increase in the fluctuation of the heave motion. This phenomenon can be attributed to our objective function, which is defined as

minimizing the average heave speed. This issue is related to fatigue and dynamic loading concerns and requires further attention in future research.

5.3. Analysis of Irregular Waves

In the controlled environment of regular waves, achieving an optimal control result is more straightforward. The predictability and uniformity of regular waves allow for a control strategy that can be finely tuned to the wave's frequency. This periodic behaviour in regular waves is helpful to the calculation of an optimal average B_{PTO} and leads to efficient control. However, the irregular waves introduce complexity due to the stochastic nature of the ocean, with many different frequencies and amplitudes present simultaneously. The control system must adapt to various conditions, and a periodic control command may no longer be adequate.

The real-world applicability of the model is proven when it is tested against these irregular wave conditions. The average significant wave height, H_{s}, spectral peak periods, T_{p}, and peakedness parameter, γ, of three sea states generated using the Jonswap spectrum are listed in Table 3.

Table 3. Irregular wave conditions [35].

	H_s (m)	T_p (s)	γ
Load 1	1.22	6	3.3
Load 2	1.98	7.5	3.3
Load 3	3.05	8.9	3.3

The relationship of forces exerted on a semi-submersible platform is depicted in Figure 9. It indicates that the wave forces experienced by the platform are partly, but not perfectly, counteracted by the PTO damping forces. When the two forces are in phase, the net force will lead to the opposite effect of motion mitigation. However, there is still a notable reduction in the overall heave motions of the platform. Figure 10 details the heave motion mitigation effect under three different load cases in irregular waves. The reduction effect across all cases suggests that the control strategy dampens the heave motion effectively. The results prove the control method's robustness and relevance for practical engineering applications. The model demonstrates its potential for real-world deployment by proving effective in these scenarios.

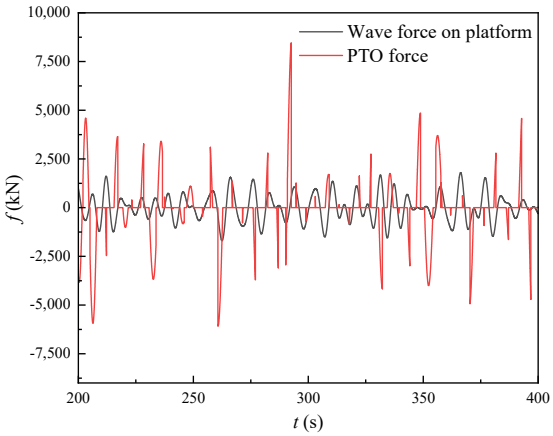

Figure 9. Time domain results of the SS-ring system under irregular waves.

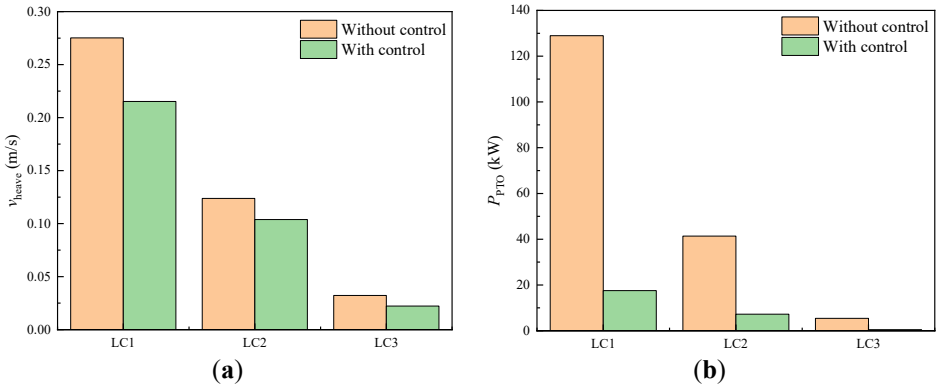

Figure 10. The control effect in irregular waves on (**a**) average heave speed and (**b**) average power absorption.

6. Conclusions

This study applies optimal declutching control to reduce wave-induced motion of a floating platform while simultaneously converting mechanical energy into electric energy. In our previous work [25], the optimisation algorithm, iteration numbers, and application scenarios based on objective functions of optimal declutching control were analysed in detail. Here, a heave ring is added to a semi-submersible (SS) floating platform as a case to study the effect of our control method on motion control.

Declutching control allows the auxiliary ring to temporarily separate from the PTO (Power Take-Off) system and stop providing damping force to the platform. The ring can gain large acceleration during the declutching period and provide a larger damping force to the platform when it is connected to the platform again. The optimal control algorithm calculates the control command to minimise platform motion.

The heave motion of the platform v_{heave} is reduced with the optimal declutching control in regular waves and irregular sea conditions. Since the auxiliary ring is accelerated occasionally, the energy absorbed by the PTO system P_{PTO} is increased simultaneously as a "by-product". v_{heave} is reduced at maximum by 30% in different wave frequencies. These two performance indices have a high cross-correlation coefficient *r* of nearly 1, indicating a positive linear relationship between the two indices. From the energy point of view, the kinetic energy of the platform is converted to the energy absorbed by the PTO system. From the phase point of view, the ring can "catch up" the wave when declutching control is activated and the PTO damping is offloaded. Additionally, the average B_{PTO} is reduced during declutching, so the angular velocity of the ring increases.

A key advantage of the proposed method is that it hardly requires additional power input, as the device harnesses the wave energy present in the system. This significantly differs from the high-cost active control methods that typically rely on external power sources. Moreover, our approach enables phase control, which can be realised by opening or closing a valve within the multi-body system. This allows for precise tuning of the wave force acting on the bodies, resulting in more effective motion control and minimal power demand. Furthermore, the extra power generated by the PTO system can be stored and utilised for other purposes.

The effectiveness of optimal declutching control is influenced by three factors, the wave frequency, the damping coefficient, and the mass ratio between the ring and the platform. In future work, these aspects could be optimised for improved design. The concept is not limited to heave rings or floating platforms. It can be extended to various scenarios of multi-body systems, such as wave attenuators, for controlling wave-induced motions.

Author Contributions

S.-R.Y.: Conceptualisation, Data Curation, Formal analysis, Investigation, Methodology, Software, Validation, Visualisation, Writing—Original Draft. Z.-M.Y.: Conceptualisation, Formal analysis, Methodology, Resources, Software, Supervision, Writing—Review & Editing. A.I.: Supervision, Validation, Writing—review & editing.

Ethics Statement

Not applicable.

Informed Consent Statement

Not applicable.

Data Availability Statement

The datasets generated during and/or analysed during the current study are available from the corresponding author on request.

Funding

This work is part of the International Excellent Young Scientists Programme funded by the National Natural Science Foundation of China (NSFC) with Grant No. W2432030.

Declaration of Competing Interest

The authors declare that they have no known competing financial interests or personal relationships that could have appeared to influence the work reported in this paper.

References

1. Musial W, Butterfield S, Boone A. Feasibility of floating platform systems for wind turbines. In Proceedings of the 42nd AIAA Aerospace Sciences Meeting and Exhibit, Reno, Nevada, 5–8 January 2004; p. 1007.
2. DNVGL. DNVGL-RP-0286 Coupled analysis of floating wind turbines. In *Recommend Practice DNVGL-RP-0286*; DNV GL: Oslo, Norway, 2019.
3. Cermelli C, Roddier D, Aubault A. WindFloat: A floating foundation for offshore wind turbines—Part II: hydrodynamics analysis. In Proceedings of the International Conference on Offshore Mechanics and Arctic Engineering, Honolulu, HI, USA, 31 May–5 June 2009; pp. 135–143. Available online: http://asmedigitalcollection.asme.org/OMAE/proceedings-pdf/OMAE2009/43444/135/4574663/135_1.pdf (accessed on 16 February 2010).
4. Sudhakar S, Nallayarasu S. Influence of heave plate on hydrodynamic response of spar. In Proceedings of the International Conference on Offshore Mechanics and Arctic Engineering, Rotterdam, The Netherlands, 19–24 June 2011; pp. 437–447. Available online: http://asmedigitalcollection.asme.org/OMAE/proceedings-pdf/OMAE2011/44335/437/4559229/437_1.pdf (accessed on 31 October 2011).
5. Lopez-Pavon C, Souto-Iglesias A. Hydrodynamic coefficients and pressure loads on heave plates for semi-submersible floating offshore wind turbines: A comparative analysis using large scale models. *Renew Energy* **2015**, *81*, 864–881. doi:10.1016/j.renene.2015.04.003.
6. Bearman P, Branković M. Experimental studies of passive control of vortex-induced vibration. *Eur. J.Mech. B/Fluids* **2004**, *23*, 9–15. doi:10.1016/j.euromechflu.2003.06.002.
7. Zhou T, Razali SFM, Hao Z, Cheng L. On the study of vortex-induced vibration of a cylinder with helical strakes. *J. Fluids Struct.* **2011**, *27*, 903–917. doi:10.1016/j.jfluidstructs.2011.04.014.
8. Rashidi S, Hayatdavoodi M, Esfahani JA. Vortex shedding suppression and wake control: A review. *Ocean. Eng.* **2016**, *126*, 57–80. doi:10.1016/j.oceaneng.2016.08.031.
9. Assi GRS, Crespi T, Gharib M. Novel geometries of serrated helical strakes to suppress vortex-induced vibrations and reduce drag. *Appl. Ocean. Res.* **2022**, *120*, 103034. doi:10.1016/j.apor.2021.103034.
10. Downie MJ, Graham JMR, Hall C, Incecik A, Nygaard I. An experimental investigation of motion control devices for truss spars. *Mar. Struct.* **2000**, *13*, 75–90.
11. Montasir OA, Kurian VJ. Effect of slowly varying drift forces on the motion characteristics of truss spar platforms. *Ocean. Eng.* **2011**, *38*, 1417–1429. doi:10.1016/j.oceaneng.2011.07.007.
12. Lackner MA, Rotea MA. Passive structural control of offshore wind turbines. *Wind. Energy* **2011**, *14*, 373–388. doi:10.1002/we.426.
13. Coudurier C, Lepreux O, Petit N. Passive and semi-active control of an offshore floating wind turbine using a tuned liquid column damper. *IFAC-PapersOnLine* **2015**, *48*, 241–247. doi:10.1016/j.ifacol.2015.10.287.
14. Hokmabady H, Mojtahedi A, Mohammadyzadeh S, Ettefagh MM. Structural control of a fixed offshore structure using a new developed tuned liquid column ball gas damper (TLCBGD). *Ocean. Eng.* **2019**, *192*, 106551. doi:10.1016/j.oceaneng.2019.106551.
15. Du J, Zhang D, Zhang Y, Xu K, Chang A, Zhao S. Design and comparative analysis of alternative mooring systems for offshore floating photovoltaics arrays in ultra-shallow water with significant tidal range. *Ocean. Eng.* **2024**, *302*, 117649. doi:10.1016/J.OCEANENG.2024.117649.
16. Jonkman JM. Influence of Control on the Pitch Damping of a Floating Wind Turbine. 2008. Available online: http://www.osti.gov/bridge (accessed on 01 March 2008).
17. Skaare B, Nielsen FG, Hanson TD, Yttervik R, Havmøller O, Rekdal A. Analysis of measurements and simulations from the Hywind Demo floating wind turbine. *Wind Energy* **2015**, *18*, 1105–1122. doi:10.1002/we.1750.
18. Skaare B, Hanson TD, Nielsen FG, Yttervik R, Hansen AM, Thomsen K, et al. Integrated dynamic analysis of floating offshore wind turbines. *Eur. Wind. Energy Conf. Exhib.* **2007**, *3*, 1929–1939.
19. Park S, Lackner MA, Pourazarm P, Rodriguez Tsouroukdissian A, Cross-Whiter J. An investigation on the impacts of passive and semi-active structural control on a fixed-bottom and a floating offshore wind turbine. *Wind Energy* **2015**, *22*, 1451–1471.
20. Truong HVA, Dang TD, Vo CP, Ahn KK. Active control strategies for system enhancement and load mitigation of floating offshore wind turbines: A review. *Renew. Sustain. Energy Rev.* **2022**, *170*, 112958. doi:10.1016/j.rser.2022.112958.
21. Yang Z, Li Y. Active vertical vane control for stabilizing platform roll motion of floating offshore turbines. *Wind Energy* **2018**, *21*, 997–1010. doi:10.1002/we.2209.
22. Wu Z, Li Y. Hybrid model predictive control of floating offshore wind turbines with artificial muscle actuated mooring lines. *J. Dyn. Syst. Meas. Control. Trans. ASME* **2022**, *144*, 051003. doi:10.1115/1.4053429.

23. Khedkar K, Nangia N, Thirumalaisamy R, Bhalla APS. The inertial sea wave energy converter (ISWEC) technology: Device-physics, multiphase modeling and simulations. *Ocean. Eng.* **2021**, *229*, 108879. doi:10.1016/j.oceaneng.2021.108879.
24. Hu L, Zhang M, Yu X, Yuan ZM, Li W. Real-time control of ship's roll motion with gyrostabilisers. *Ocean. Eng.* **2023**, *285*, 115348. doi:10.1016/j.oceaneng.2023.115348.
25. Yu SR, Zhang M, Zhang DQ, Yuan ZM. Optimal declutching control of hinged multiple floating bodies. *Ocean. Eng.* **2024**, *306*, 117992. doi:10.1016/j.oceaneng.2024.117992.
26. Robertson A, Jonkman J, Masciola M, Song H, Goupee A, Coulling A, et al. Definition of the Semisubmersible Floating System for Phase II of OC4, 2014. Available online: www.nrel.gov/publications (accessed on 01 September 2014).
27. Chakrabarti S, Barnett J, Kanchi H, Mehta A, Yim J. Design analysis of a truss pontoon semi-submersible concept in deep water. *Ocean. Eng.* **2007**, *34*, 621–629. doi:10.1016/j.oceaneng.2006.03.012.
28. Ma R, Bi K, Hao H. Mitigation of heave response of semi-submersible platform (SSP) using tuned heave plate inerter (THPI). *Eng. Struct.* **2018**, *177*, 357–373. doi:10.1016/j.engstruct.2018.09.085.
29. Muliawan MJ, Karimirad M, Moan T. Dynamic response and power performance of a combined Spar-type floating wind turbine and coaxial floating wave energy converter. *Renew Energy* **2013**, *50*, 47–57. doi:10.1016/j.renene.2012.05.025.
30. Cummins WE. *The Impulse Response Function and Ship Motions*, *Report 1661*, *Research and Development Report*; Department of the Navy, David W. Taylor Model Basin, Hydromechanics Laboratory: Washington, DC, USA, 1962.
31. Perez T, Fossen TI. A Matlab toolbox for parametric identification of radiation-force models of ships and offshore structures. *Model. Identif. Control.* **2009**, *30*, 1–15. doi:10.4173/mic.2009.1.1.
32. Ringwood JV, Bacelli G, Fusco F. Energy-maximizing control of wave-energy converters: The development of control system technology to optimize their operation. *IEEE Control Syst.* **2014**, *34*, 30–55. doi:10.1109/MCS.2014.2333253.
33. Yuan ZM, Incecik A, Dai S, Alexander D, Ji CY, Zhang X. Hydrodynamic interactions between two ships travelling or stationary in shallow waters. *Ocean. Eng.* **2015**, *108*, 620–635. doi:10.1016/j.oceaneng.2015.08.058.
34. Zhang D, Yuan ZM, Du J, Li H. Hydrodynamic modelling of large arrays of modularized floating structures with independent oscillations. *Appl. Ocean. Res.* **2022**, *129*, 103371. doi:10.1016/j.apor.2022.103371.
35. Yim SCS, Nakhata T, Huang ET. Coupled nonlinear barge motions, part II: Stochastic models and stability analysis. *J. Offshore Mech. Arct. Eng.* **2005**, *127*, 83–95. doi:10.1115/1.1884617.